Supporting Information

Biocompatible Glyconanoparticles by Grafting of Sophorolipid Monolayers on Monodisperse Iron Oxide Nanoparticles

Andrea Lassenberger,[a,b] Andrea Scheberl,[a] Krishna Chaithanya Batchu,[b] Viviana Cristiglio,[b] Isabelle Grillo,[b] Daniel Hermida Merino,[c] Erik Reimhult,[a,*] Niki Baccile[d,*]

[a]University of Natural Resources and Life Sciences Vienna, Institute for Biologically inspired materials, Department of Nanobiotechnology, Muthgasse 11/II, 1190 Vienna, Austria
*erik.reimhult@boku.ac.at

[b]Institut Laue-Langevin, 71 Avenue des Martyrs, 38042 Grenoble Cedex 9, France

[c]ESRF – The European Synchrotron, 71 Avenue des Martyrs, 38042 Grenoble Cedex 9, France

[d]Sorbonne Université, Centre National de la Recherche Scientifique, Laboratoire de Chimie de la Matière Condensée de Paris, LCMCP, F-75005 Paris, France

*erik.reimhult@boku.ac.at; niki.baccile@upmc.fr

Materials

Iron(0)pentacarbonyl (99,99 % trace metal basis), oleic acid (≥ 93 % technical grade), dioctyl ether (> 99 %), iron (III) chloride hexahydrate (≥ 98 %), sodium oleate (> 99 %), dopamine hydrochloride (≥ 98 %), sulfuric acid (95 - 98 %), sodium nitrite (≥ 99 %), 4-methyl-morpholine (99 % ReagentPlus), (1-cyano-2-ethoxy-2-oxoethylidenaminooxy)-dimethylamino-morpholino-carbenium hexafluorophosphate (COMU, 97 %), hydrochloric acid (37 % ACS reagent), sodium hydroxide (99 %), phosphate buffered saline (PBS 10x concentrate BioPerformance certified), PenStrep, Dulbecco's Modified Eagle's Medium, Agarose (BioReagent), PrestoBlue® Cell Viability assay, Ferrozin (3-(2-pyridyl)-5,6-diphenyl-1,2,4-triazine-4′,4′′-disulfonic acid sodium salt, ≥ 98 %), iron(III)chloride (≥ 99 %), neocuproine (≥ 98 %), ascorbic acid (≥ 98 %), ammoniumacetate (≥ 98 %), Bradford Reagent, bovine serum albumin (≥ 98.0 %), cell culture media RPMI-1460, HEPES (≥ 99.5 %), fetal calf serum (FCS) and acetonitrile (HPLC Plus, ≥ 99.9 %) were purchased from Sigma Aldrich ; DMF (> 99,9 % ACS reagent), $CHCl_3$ (≥ 99.5 % containing 100-200ppm amylenes as stabilizer), n-hexane (≥ 95 % chromasolv plus for HPLC), and 1-butanol (≥ 99 %) were obtained from Carl Roth. Ultrapure Milli-Q water (Millipore USA, R = 18 MΩcm) was used for all experiments.

Table S1. Iron oxide cores synthesized using a slight modification of the method developed by Hyeon et al.[1] Core size was controlled by varying the ratio of precursor to surfactant.

NP diameter (nm)	$Fe(CO)_5$: OA (molar ratio)
3.1 ± 0.3	1:1.6
4.6 ± 0.3	1:1.9
10.9 ± 0.3	1:4

Characterization of nitrocatechol-glyco ligands (SL-NDA)

In addition to the extraction-purification protocol described in the manuscript, we applied a further purification step for the product to remove residual solvents and coupling agents. SL-NDA was isolated by HPLC using a stationary phase, HyperSep C18 cartridge (500 mg, Thermo Scientific, USA). The reaction mixture was dissolved in H_2O/ acetonitrile (ACN) (95:5) and applied to the cartridge that was pre-equilibrated with 25 ml H_2O/ACN (95:5). The cartridge was first eluted with 25 ml H_2O/ACN (90:10) and then with 25 ml H_2O/ACN (70:30) to elute nitrodopamine and other polar contaminants. In the final step the synthesized SL-NDA was eluted by applying 50 ml pure ACN. The purified fraction from the final step was taken to dryness under an N_2 stream.

Coupling was verified by ^1H solution NMR in Figure S1, which reports both the SL-NDA, SL and NDA ^1H NMR spectra. The attribution of the major peaks, as well as their relative integration, are also reported in the Table in Figure S1a. The H signals of the catechol group in NDA are found at H_a= 7.55 ppm, H_b= 6.72 ppm, while H_c= 3.04 ppm.[2, 3] In particular, we observe the expected shift of H_d from 3.04 ppm (α-CH_2 in amine) to 3.47 ppm (α-CH_2 in amide), as classically found in ethylene oleylamides and verified here by the correlation between H_c and H_d in the corresponding COSY pattern (Figure S1 b, c). We also observe the α-CH_2 (H_2) shift from 2.30 ppm in SL(COOH, acid) to H_2^*= 2.18 ppm in SL(CONR, amide).

Integration values suggest a 1:1 ratio between SL and NDA. Unreacted sophorolipids between 10 and 20 mol % should not be excluded.

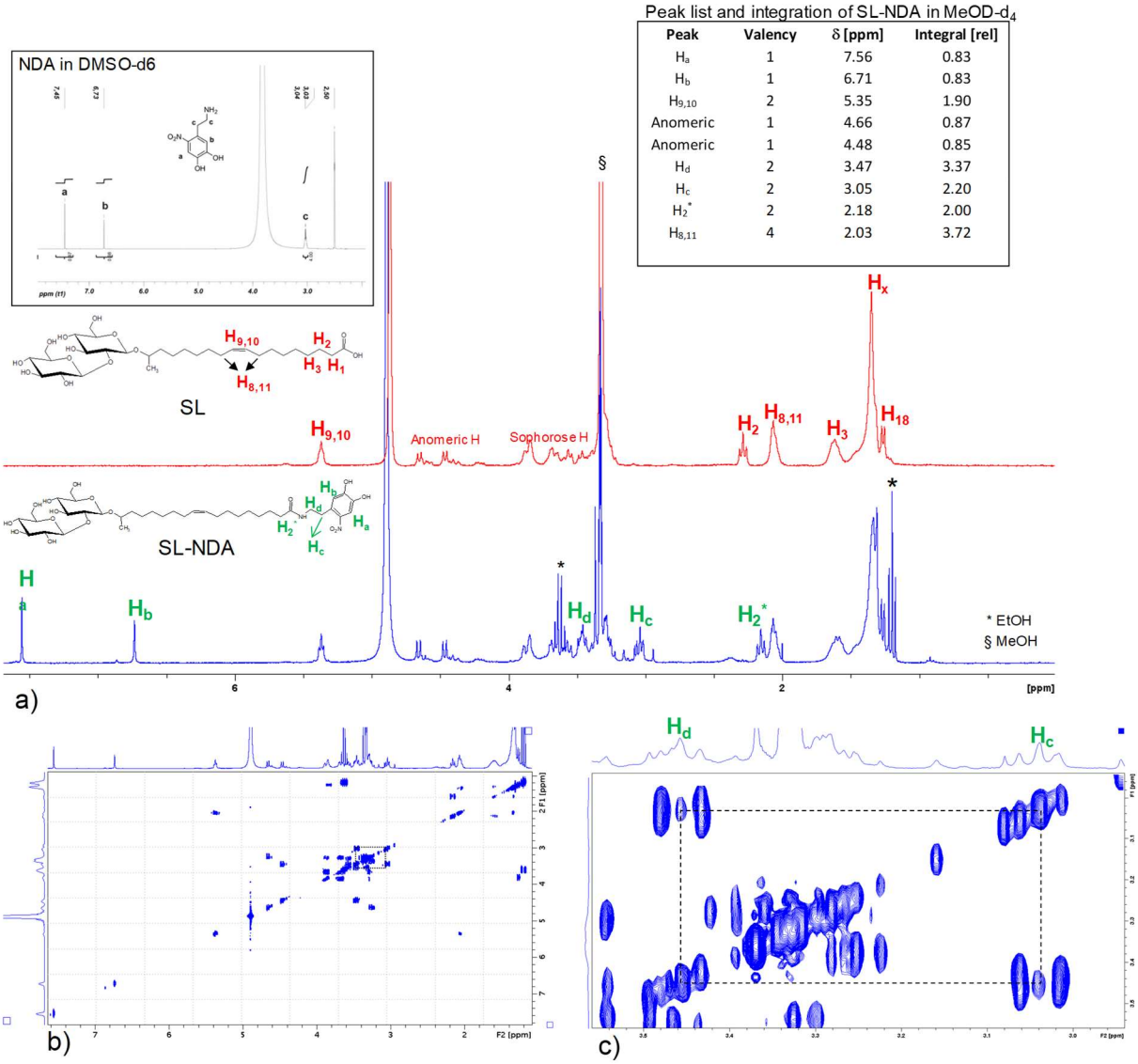

Figure S1. a) ^{1}H NMR spectra of SL-NDA ligand in MeOD containing residual COMU coupling agent and solvents.[4] b-c) Corresponding COSY 2D NMR of SL-NDA. In c), the correlation between H_c and H_d in SL-NDA is highlighted, demonstrating the amide coupling.

TEM Analysis of OA-capped IONP

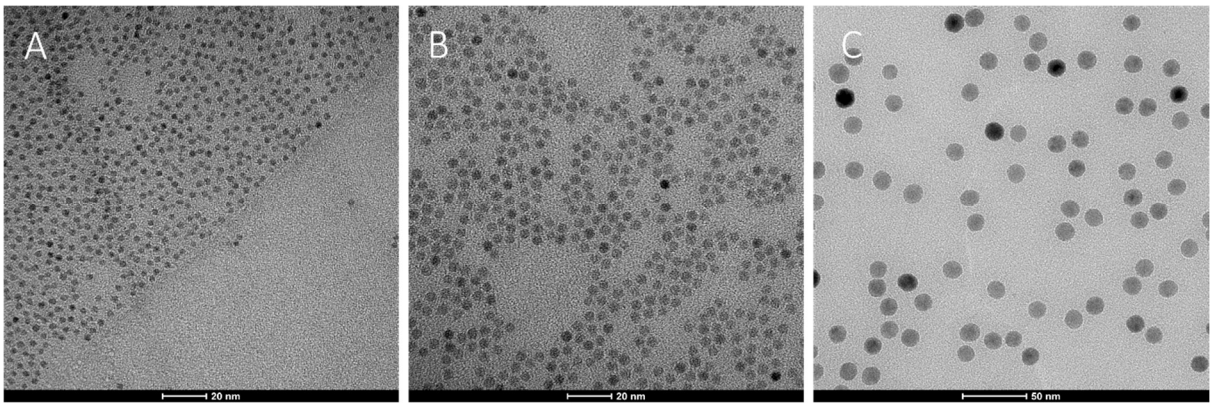

Figure S2. OA-capped IONP sized A) 3.1 ± 0.3 nm, B) 4.6 ± 0.3 nm and C) 14.1 ± 0.9 nm.

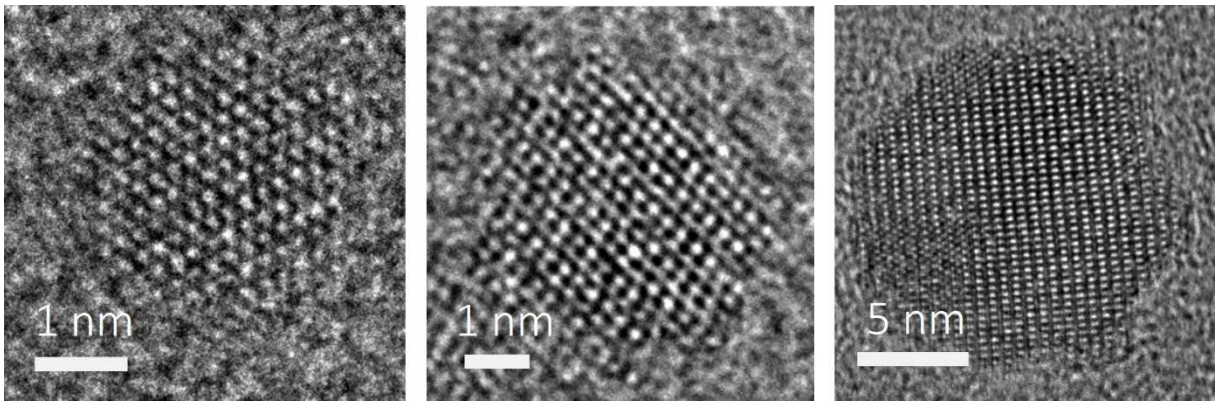

Figure S3. HR-TEM of SL-NDA coated IONP of core sizes 3.1, 4.6 and 14.1 nm (from left to right) showing single crystallinity without defects. The distorted shape of the 14.1 nm NPs is due to radiation damage under the electron beam.

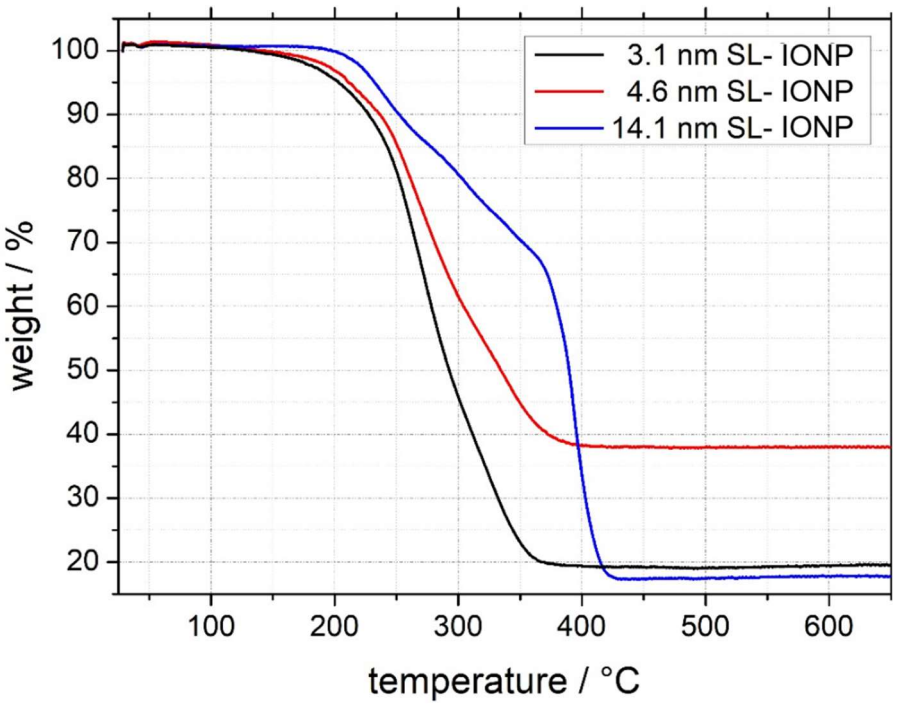

Figure S4. TGA data of 3.1 nm SL-IONP (black), 4.6 nm SL-IONP (red) and 14.1 nm SL-IONP (blue) purified by membrane centrifugation (50 kDa MWCO). The organic mass loss for 4.6 nm SL-IONP up to 500 °C is much smaller

than that for 3.1 nm and 14.1 nm SL-IONP, indicating that the latter samples contained a larger excess of unbound ligand that could not be sufficiently removed by dialysis or membrane centrifugation.

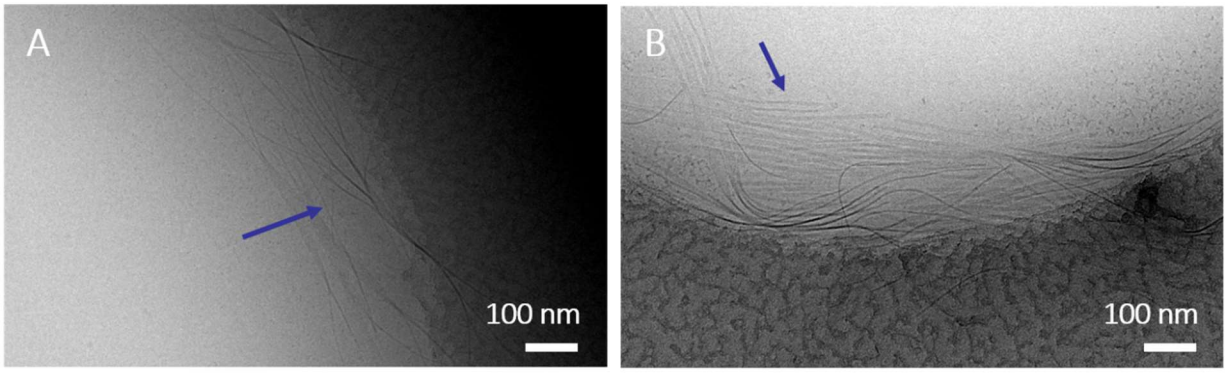

Figure S5. Cryo-TEM images of a 5 mg/mL SL-NDA solution in D_2O. The blue arrows indicate fibrillary structures and fibers merging into flat morphologies. A) and B) are micrographs from the same sample at different locations.

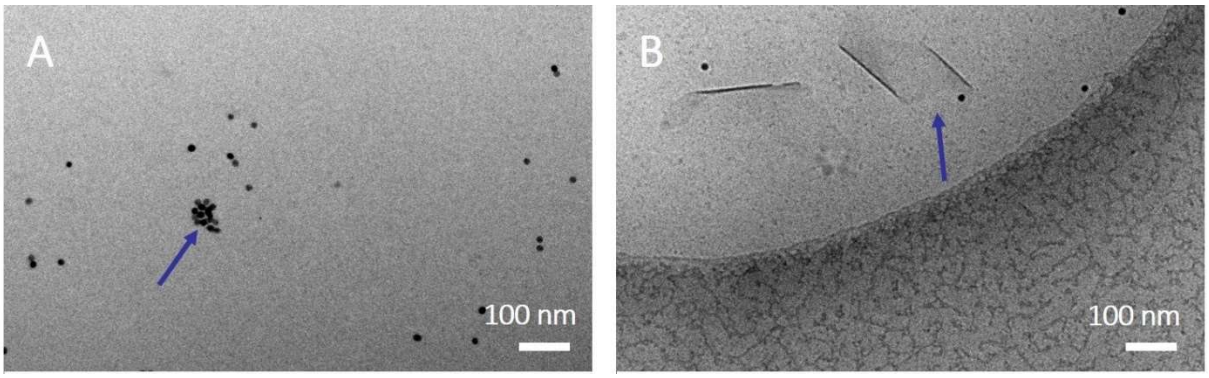

Figure S6. Cryo-TEM images of 14.1 nm SL-IONP in D_2O. The blue arrow in **A)** shows small NP agglomerates next to well-dispersed core-shell NPs and the arrow in **B)** indicates flat self-assembled morphologies.

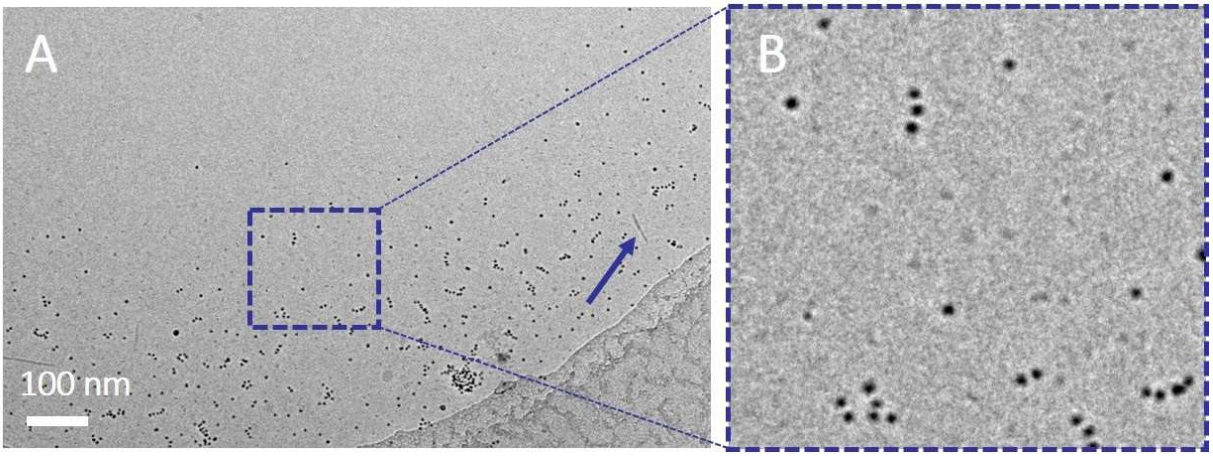

Figure S7. Cryo-TEM images of 4.6 nm SL-IONP in D_2O. The blue arrow in **A)** indicates a small residue of fibrillary structures of the excess ligand present. However, the amount of such objects found was much smaller than in the 14.1 nm SL-IONP sample. **B)** Enlarged region of **A)** showing that the majority of SL-IONP in this sample was well-dispersed.

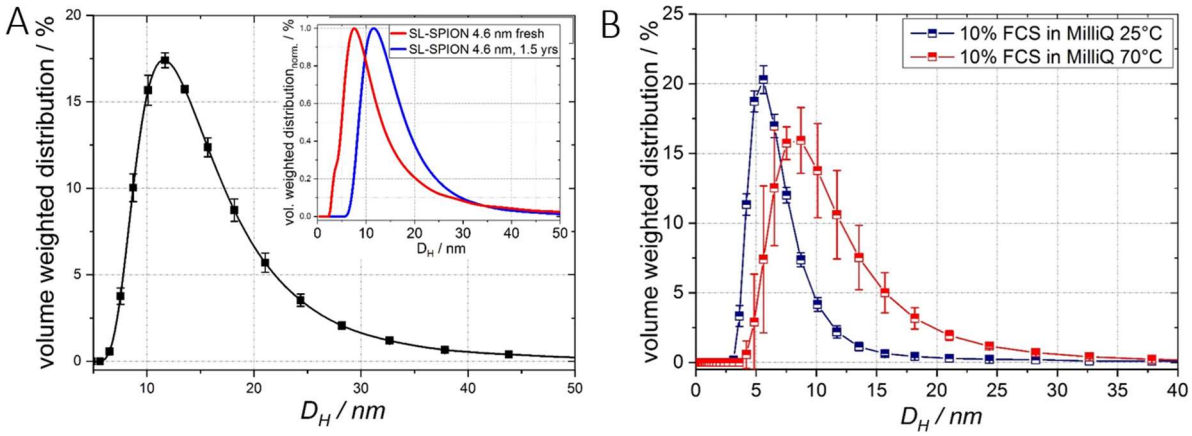

Figure S8. A) Volume weighted DLS hydrodynamic diameter of 4.6 nm SL-IONP in water at 20 °C. Inset: long-term stability of SL-IONP 4.6 nm freshly dissolved (red) and the same sample after 1.5 years storage at 25°C (blue) **B)** Volume weighted DLS hydrodynamic diameters of 10 % FCS in Milli-Q at 20 °C (blue) and 70°C (red), measured at 30 min equilibration time each.

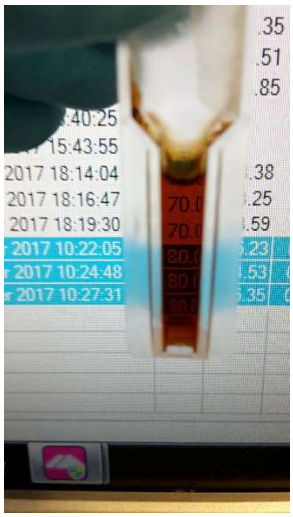

Figure S9. Image of 4.6 nm SL-IONP after temperature cycling in MilliQ and 10 % FCS. The dispersion is clear and does not show any sign of visible aggregation.

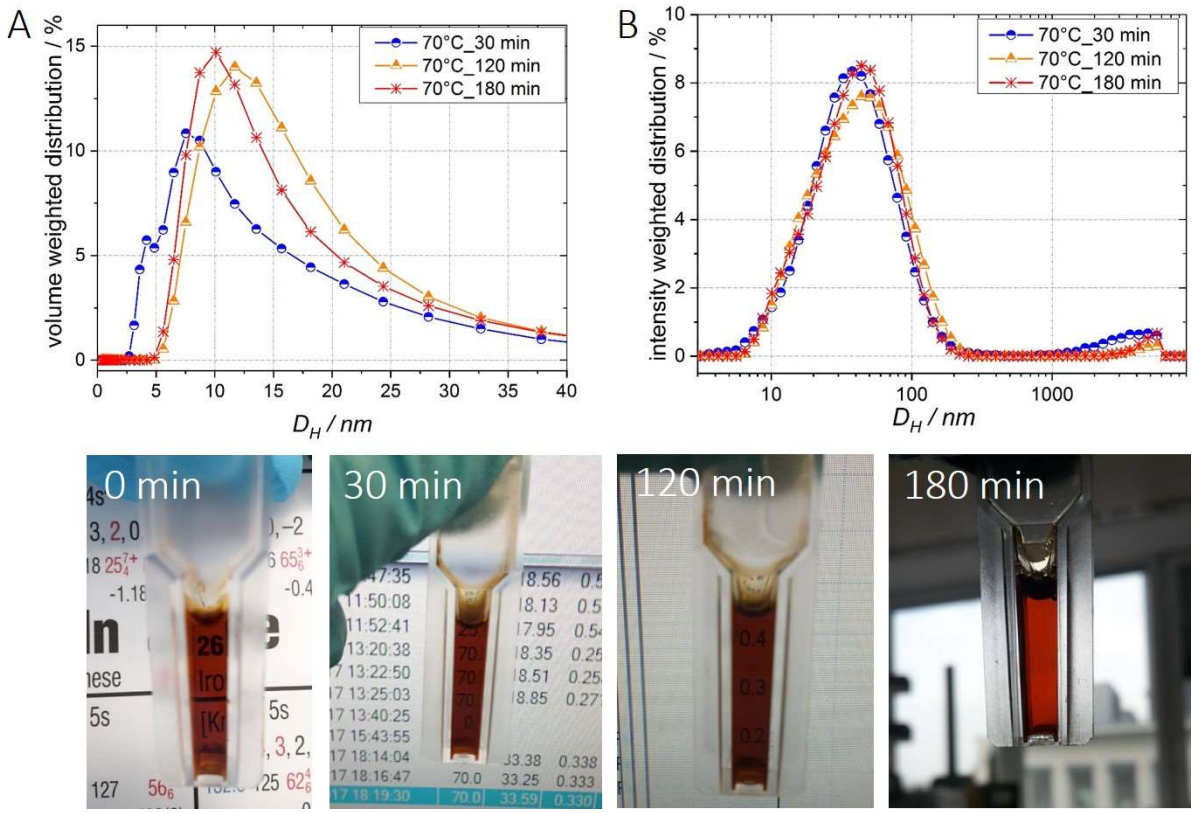

Figure S10. Aggregation behavior of 4.6 nm SL-IONP in Milli-Q and 10 % FCS. NPs were heated to 70 °C and DLS data was measured after 60 (blue), 120 (orange) and 180 min (red). **A)** Volume weighted hydrodynamic diameters $\boldsymbol{D_H}$ and **B)** intensity weighted hydrodynamic diameters $\boldsymbol{D_H}$. A slight increase in size could be observed but no aggregation took place as evident from the pictures in the lower panel showing clear dispersions of IONP without visible aggregation.

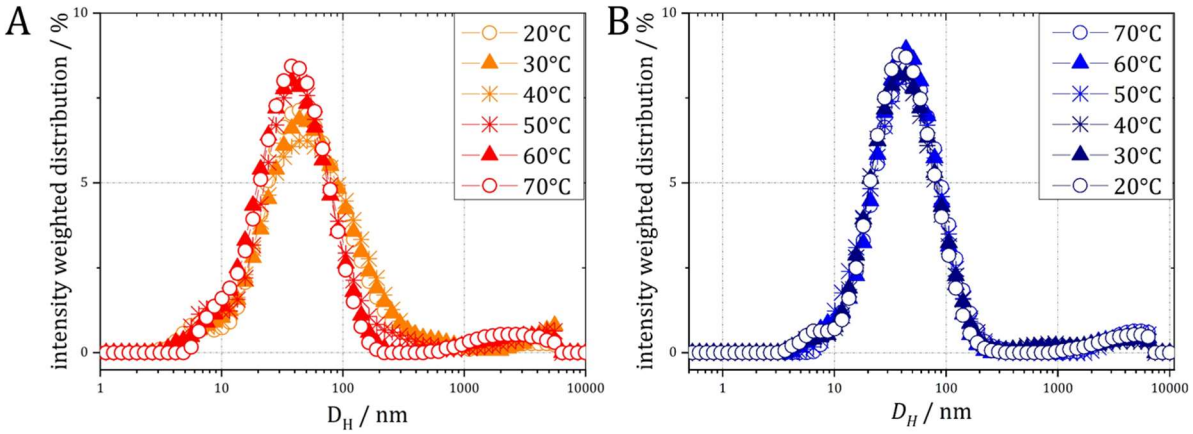

Figure S 11. Intensity-weighted hydrodynamic diameters $\boldsymbol{D_H}$ of 4.6 nm SL-IONP dispersed in water with 10 % FCS heated from A) 20 °C to 70 °C and B) cooled from 70 °C to 20 °C with 3 minutes equilibration time at each temperature.

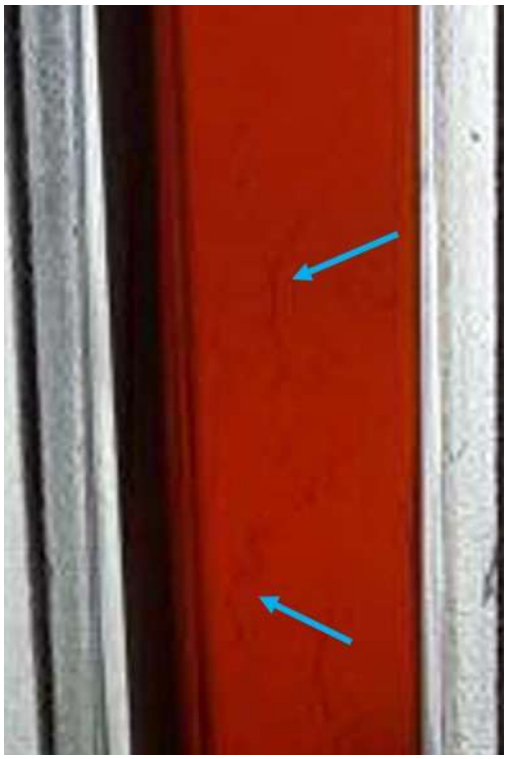

Figure S12. Enlarged Figure S10 showing 4.6 nm SL-IONP and FCS after 180 min heating at 70 °C. The blue arrows indicate aggregated protein.

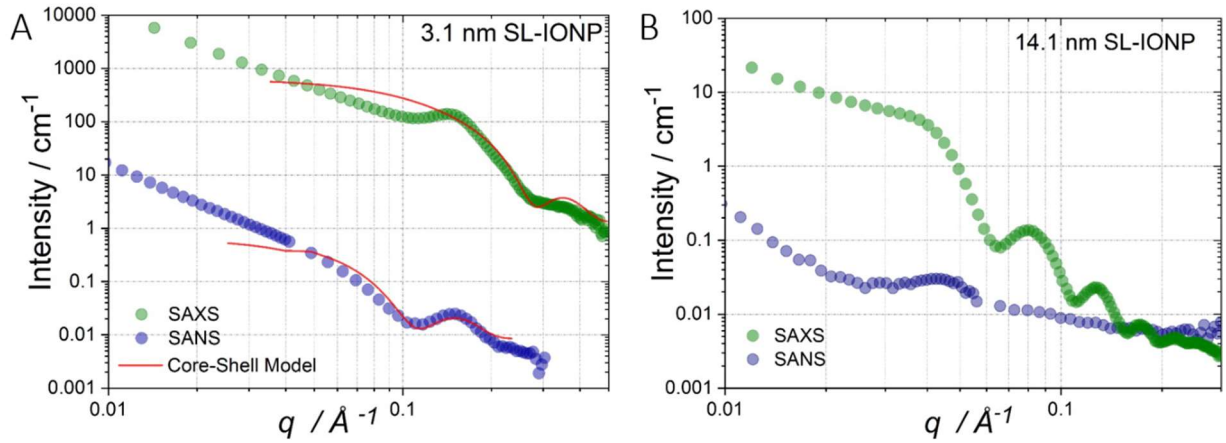

Figure S13. SAXS and SANS profiles for **A)** 3.1 nm SL-IONP and **B)** 14.1 nm SL-IONP in D_2O. Both samples show strong interactions at low q originating from excess ligand present in the samples.

References

1. Hyeon, T.; Lee, S. S.; Park, J.; Chung, Y.; Na, H. B., Synthesis of Highly Crystalline and Monodisperse Maghemite Nanocrystallites without a Size-Selection Process. *J. Am. Chem. Soc.* 2001, *123* (51), 12798-12801.

2. Kurzhals, S.; Zirbs, R.; Reimhult, E., Synthesis and Magneto-Thermal Actuation of Iron Oxide Core–PNIPAM Shell Nanoparticles. *ACS Appl. Mat. Interfaces* 2015, *7* (34), 19342-19352.

3. Bixner, O.; Lassenberger, A.; Baurecht, D.; Reimhult, E., Complete Exchange of the Hydrophobic Dispersant Shell on Monodisperse Superparamagnetic Iron Oxide Nanoparticles. *Langmuir* 2015, *31* (33), 9198-9204.

4. El-Faham, A.; Albericio, F., COMU: A third generation of uronium-type coupling reagents. *J. Pept. Sci.* 2010, *16*, 6-9.